Article

Adaptative survival of Aspergillus fumigatus to echinocandins arises from cell wall remodeling beyond β−1,3-glucan synthesis inhibition

Malitha C. Dickwella Widanage[1,10,11], Isha Gautam[1,11], Daipayan Sarkar[2], Frederic Mentink-Vigier [3], Josh V. Vermaas [2,4], Shi-You Ding [5], Andrew S. Lipton [6], Thierry Fontaine[7], Jean-Paul Latgé[8], Ping Wang [9] & Tuo Wang [1] ✉

Antifungal echinocandins inhibit the biosynthesis of β−1,3-glucan, a major and essential polysaccharide component of the fungal cell wall. However, the efficacy of echinocandins against the pathogen *Aspergillus fumigatus* is limited. Here, we use solid-state nuclear magnetic resonance (ssNMR) and other techniques to show that echinocandins induce dynamic changes in the assembly of mobile and rigid polymers within the *A. fumigatus* cell wall. The reduction of β−1,3-glucan induced by echinocandins is accompanied by a concurrent increase in levels of chitin, chitosan, and highly polymorphic α−1,3-glucans, whose physical association with chitin maintains cell wall integrity and modulates water permeability. The rearrangement of the macromolecular network is dynamic and controls the permeability and circulation of the drug throughout the cell wall. Thus, our results indicate that echinocandin treatment triggers compensatory rearrangements in the cell wall that may help *A. fumigatus* to tolerate the drugs' antifungal effects.

Invasive *Aspergillus* infections have high and increasing occurrence and mortality among immunocompromised and immunocompetent patients[1–3], including, more recently, critically ill individuals suffering from SARS-CoV-2 infections[4,5]. There are currently a few antifungal agents available, with often therapeutic failures and a recently observed increase in drug resistance[6–9]. The cell wall is a prominent target for the selection of very specific antifungal drugs. Therefore, echinocandins, such as caspofungin and micafungin, have been

approved for clinical applications[10–12]. These cyclic hexapeptides, which possess modifiable aliphatic tails (Fig. 1a), inhibit the biosynthesis of β-1,3-glucan, a major and essential structural polysaccharide in the fungal cell wall[10,13].

As an effective fungicide for *Candida* species, echinocandins are being used as preferred agents for treating invasive candidiasis[14,15]. However, echinocandins only have relatively low efficacy in vitro and in vivo against *A. fumigatus*, the most ubiquitous airborne fungal

[1]Department of Chemistry, Michigan State University, East Lansing, MI, USA. [2]MSU-DOE Plant Research Laboratory, East Lansing, MI, USA. [3]National High Magnetic Field Laboratory, Tallahassee, FL, USA. [4]Biochemistry and Molecular Biology, Michigan State University, East Lansing, MI, USA. [5]Department of Plant Biology, Michigan State University, East Lansing, MI, USA. [6]Environmental Molecular Sciences Laboratory, Pacific Northwest National Laboratory, Richland, WA, USA. [7]Institut Pasteur, Université Paris Cité, INRAE, USC2019, Unité Biologie et Pathogénicité Fongiques, F-, 75015 Paris, France. [8]Institute of Molecular Biology and Biotechnology, University of Crete, Heraklion, Greece. [9]Departments of Microbiology, Immunology and Parasitology, Louisiana State University Health Sciences Center, New Orleans, LA, USA. [10]Present address: National High Magnetic Field Laboratory, Tallahassee, FL, USA. [11]These authors contributed equally: Malitha C. Dickwella Widanage, Isha Gautam. ✉e-mail: wangtuo1@msu.edu
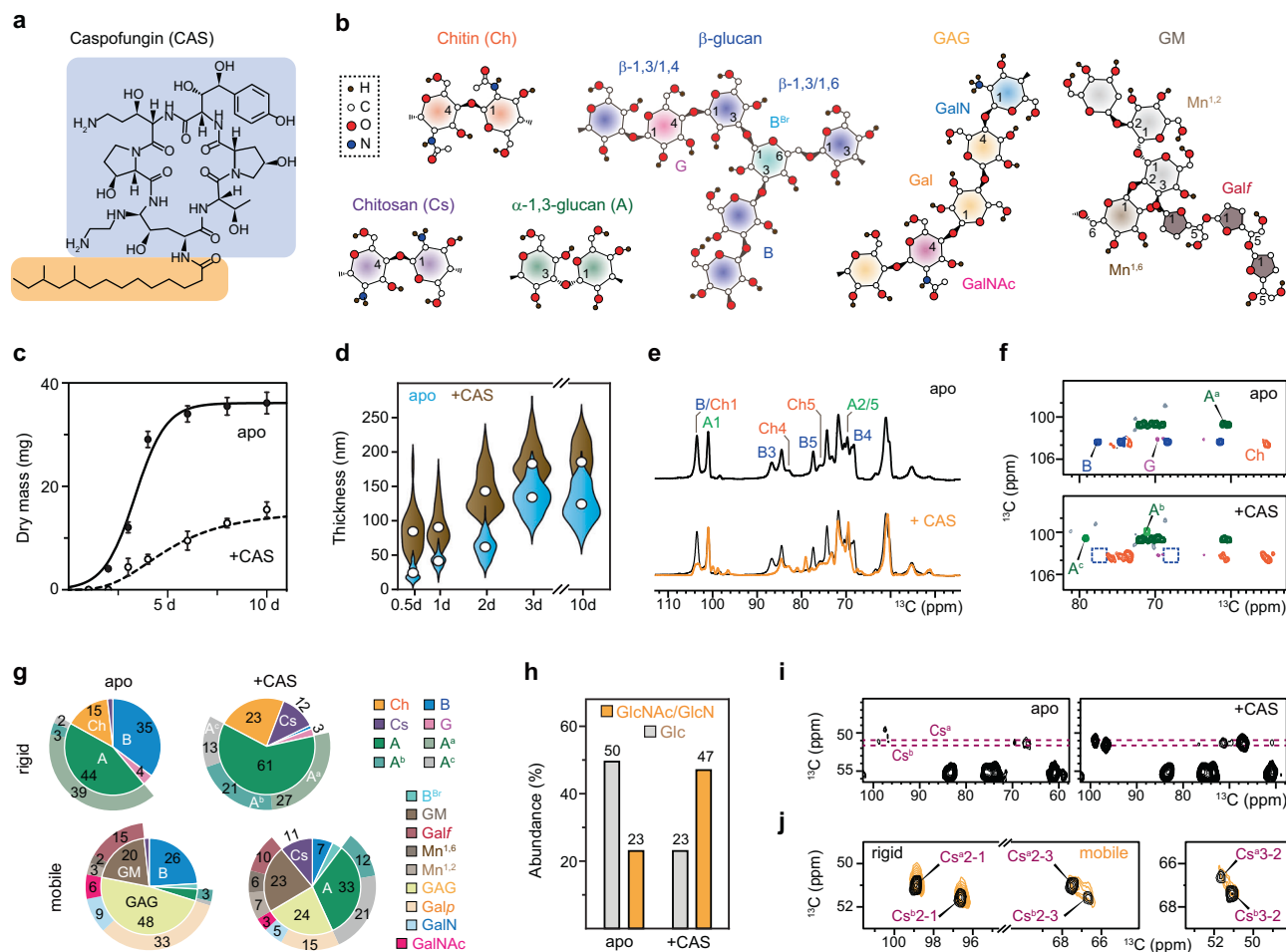
Fig. 1 | Alternation of cell wall polymer composition due to caspofungin treatment. a Chemical structure of caspofungin (CAS), highlighting the cyclic peptide in blue and the lipid component in yellow. **b** Simplified structures of fungal cell wall polysaccharides. NMR abbreviations are provided for each polysaccharide or monosaccharide unit. **c** Growth profiles of *A. fumigatus* without (apo) and with caspofungin as a change in dry mass. **d** Cell wall thickness of young and old samples determined using TEM images. Open circles: mean values. $n = 75$ for 0.5 d and 2 d apo samples. $n = 120$ for 0.5 d, 1 d, 10 d CAS-treated samples, and 2 d apo samples. $n = 200$ for other samples. **e** 1D ^{13}C CP spectra of 3-day-old *A. fumigatus* samples showing the compositional difference of rigid polysaccharides. Top: apo sample; bottom: overlay of spectra from apo (black) and caspofungin-treated (orange) samples. **f** Comparison of 2D ^{13}C-^{13}C spectra of 3-day-old cell walls. The missing peaks of β−1,3-glucans in drug-treated samples are highlighted using blue boxes. **g** Molar composition of rigid (top) and mobile (bottom) cell wall polysaccharides of 3-day-old samples estimated using volumes of resolved cross peaks in 2D ^{13}C CORD

and DP refocused J-INADEQUATE spectra. Ch: chitin, Cs: chitosan, B: β−1,3-glucan, G: β−1,4-glucose residue, A: α−1,3-glucan. For α−1,3-glucan in the rigid portion, the inner pie chart displays the total amount, while the outer circle shows the individual content of three subtypes (A^a, A^b, and A^c). B^{Br}: β-1,3,6-glucose residue (the branching point), GM: galactomannan, Gal*f*: galactofuranose, $Mn^{1,2}$: α−1,2-mannose, $Mn^{1,6}$: α−1,6-mannose. For the mobile phase, the inner pie chart depicts the total content of each polysaccharide, while the outer circle shows the monosaccharide units or subtypes. **h** Changes of the total Glc (α- and β-glucan) and GlcN/GlcNAc (chitosan and chitin) in 3-day-old cell wall using GC-MS and HPLC after acid hydrolysis. **i** Detection of two chitosan types (Cs^a and Cs^b) in drug-treated 3-day-old sample in 2D CORD spectra. **j** Presence of both chitosan forms in 3-day-old caspofungin-treated sample across both rigid fraction (black; CORD spectra) and mobile fraction (yellow; sheared refocused DP J-INADEQUATE spectra). For **c** and **d**, data are mean ± s.e. $n = 3$ replicates for **c** and $n = 200$ in 10 cells for each sample in **d**. Source data are provided as a Source Data file.

pathogen responsible for pulmonary aspergillosis, and other filamentous fungi[16,17]. Echinocandins only exert a fungistatic effect on *A. fumigatus*, causing lysis to the hyphal tips without completely preventing growth[18]. Understanding the low efficacy of these β-1,3-glucan synthase inhibitors against *A. fumigatus* would benefit therapeutic application. Given the highly dynamic nature of the fungal cell wall, which undergoes continuous modifications in response to external stresses[19–22], a plausible explanation could be the occurrence of specific compensatory mechanisms at the cell wall level promoting fungal survival by counteracting β-1,3-glucan reduction in filamentous fungi.

Recently, magic-angle spinning (MAS) ssNMR methods have unveiled the supramolecular arrangement of key polysaccharide components (Fig. 1b) within fungal cell wall architecture[23–25]. High-resolution data collected on intact *A. fumigatus* mycelia have demonstrated that α-1,3-glucan associates with chitin to form a robust

mechanical scaffold, which is dispersed within a mobile and hydrated mesh formed by branched β-glucans, and enclosed by a dynamic outer shell rich in galactomannan (GM) and galactosaminogalactan (GAG)[26,27]. This nanoscale architecture was observed to undergo significant rearrangements in response to biosynthesis deficiencies in structural polysaccharides and during morphotype transitions throughout fungal life cycles[28,29]. Such methodology has been applied now to understand the structural modifications of *A. fumigatus* cell walls when this fungus is treated with echinocandins.

Here, ssNMR and dynamic nuclear polarization (DNP) techniques, in conjunction with transmission electron microscope (TEM) and atomic force microscopy (AFM) imaging, biochemical analysis, and molecular dynamics (MD) simulations, have unveiled major unexpected structural and dynamic changes in the mycelial cell wall of *A. fumigatus* treated by echinocandins. An echinocandin-induced
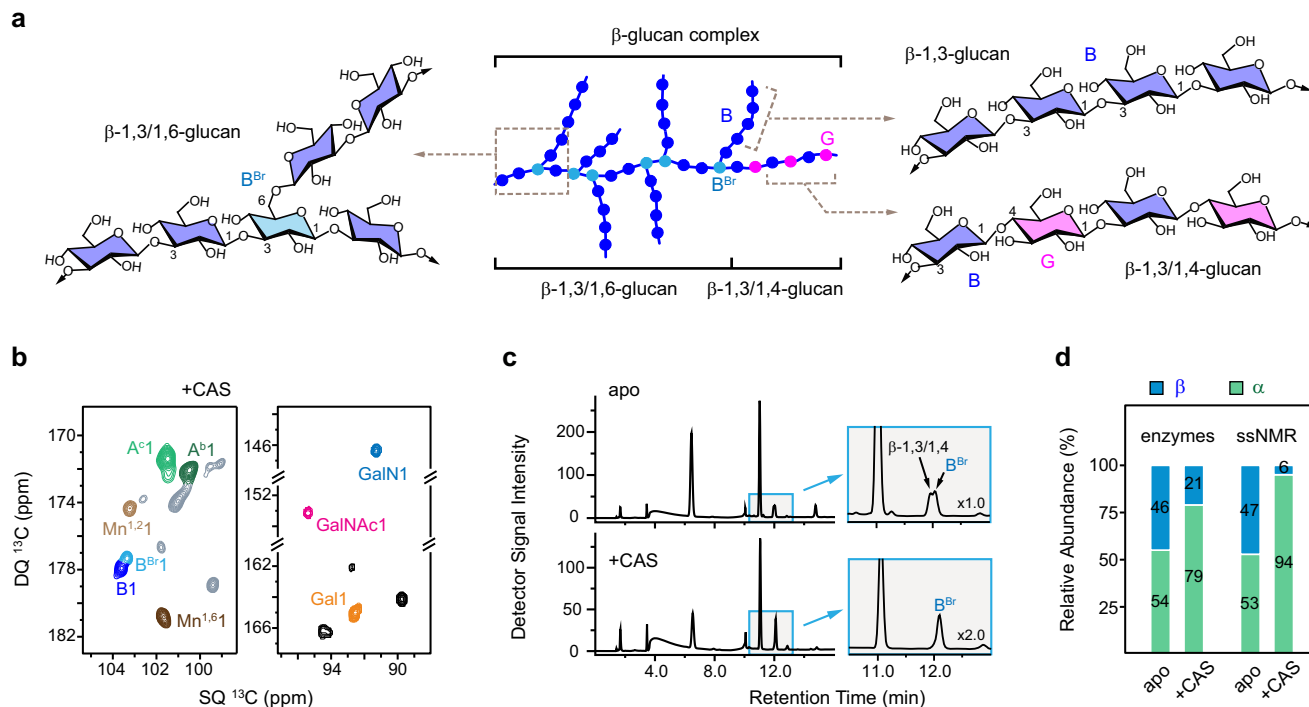
Fig. 2 | Caspofungin remodels the structures of β- and α-glucans. a Diagram illustrating the complex structure of β-glucans in *A. fumigatus* cell walls. NMR abbreviations are introduced to annotate different linkages in the main chains and branches. **b** Mobile polysaccharides detected using 2D ¹³C DP J-INADEQUATE spectrum resolving the β−1,3-linked (B) and β−1,3,6-linked (Bᴮʳ) glucose units, as well as two novel forms of α−1,3-glucans (Aᵃ and Aᵇ). **c** Qualitative analysis by HPLC shows the presence of β-glucan complex and the reduced amount of β-1,3/1,4-glucan domains after caspofungin treatment in 3-day-old cultures. **d** Percentages of α- and β-glucans in 3-day-old *A. fumigatus* samples determined by degrading the cell wall with recombinant α- and β-glucanases or using untreated cell walls by ssNMR.

augmentation of the chitin content is the first event associated with its partial deacetylation, leading to a significant amount of chitosan in the treated fungus. While only a low amount of β-glucan remains, it exhibits an atypical structure characterized by a high degree of branching. To compensate for the loss of most β-glucans, an increase in α-1,3-glucan content, along with the emergence of two novel types of semi-dynamic α-1,3-glucans, regenerates the soft matrix. The physical associations of chitosan, α-1,3-glucan, and chitin provide critical mechanical support, essential for preserving cell wall integrity. Moreover, the composition and structure of GAG and GM residing on the cell surface have been reshuffled. These compositional changes further lead to enhanced stiffness and hydrophobicity of the polymer network within the cell wall. These modifications induced by echinocandins have provided heretofore unavailable molecular insights into their limited effectiveness and defined structural paradigms for strategies to improve their efficacy.

Results

### Caspofungin alters the carbohydrate core

Under our experimental condition, the addition of 2.5 μg/mL caspofungin resulted in a notable decrease in the growth of *A. fumigatus*, reaching only 25-50% of the growth observed in the untreated culture, with variation depending on the duration of growth (Fig. 1c). Caspofungin led to a 2–3-fold increase in cell wall thickness in younger cultures (0-2 days) and a 1.5-fold increase in older cultures (3-10 days), elevating the average thickness from 133 nm to 182 nm for 3-day-old samples (Fig. 1d and Supplementary Table 1). Uniformly ¹³C, ¹⁵N-labeled *A. fumigatus* mycelia were subjected to ssNMR analysis to identify molecular-level factors driving this microscopic-scale restructuring. Initial screening by one-dimensional (1D) ¹³C spectra confirmed the reduction of the β-1,3-glucan content in the rigid structural domain (Fig. 1e). The intensity reduction of characteristic peaks of β-1,3-glucan

carbons (B3 at 86 ppm, B4 at 69 ppm, and B5 at 77 ppm), notably a 94% drop in the B3 peak, was observed in the echinocandin-treated sample. These changes were reproducibly observed across three sample batches (Supplementary Fig. 1).

Further two-dimensional (2D) ¹³C-¹³C/¹⁵N correlation spectra were acquired to resolve a large number of carbon sites in fungal glycans (Supplementary Fig. 2). As anticipated, the signals of β-1,3-glucans became almost negligible in the drug-treated cell walls (Fig. 1f). Analysis of peak volumes revealed that caspofungin decreased the β-1,3-glucan content in the rigid portion of the cell wall from 35% to 1% in 3-day-old *A. fumigatus* cultures, while the amount of chitin increased by 1.5-2-fold (Fig. 1g and Supplementary Table 2). Chemical analysis of the sugar composition through acid hydrolysis and HPLC validated the reduction in glucan content and the elevation of chitin level in the cell wall (Fig. 1h and Supplementary Table 3).

The content of chitosan, the deacetylated form of chitin, was initially minimal in the apo sample, but after caspofungin treatment, it increased to comprise 11-12% of the cell wall carbohydrates (Fig. 1i). Two distinct forms of chitosan molecules were identified, equally populated and evenly distributed across both the rigid and mobile fractions of the cell wall (Fig. 1j).

The atomic resolution of ssNMR allowed us to discern intricate structural characteristics of β-glucan complex within intact *A. fumigatus* cell walls (Fig. 2a). This includes spectroscopic identification of glucopyranose residues bearing β-1,3, β-1,3,6, and β-1,4 linkages, with a particular focus on distinguishing the branching points (Bᴮʳ) from the predominant linear chains (Fig. 2b and Supplementary Fig. 2c). The residual β-glucan surviving caspofungin treatment was hyperbranched through many β-1,3,6-linkages while its content of β-1,3/1,4-linked sequence was lower (Fig. 2c and Supplementary Fig. 3). These results show that the β-1,3/1,4-linked oligosaccharides are bound to the β-1,3 linear glucans targeted by
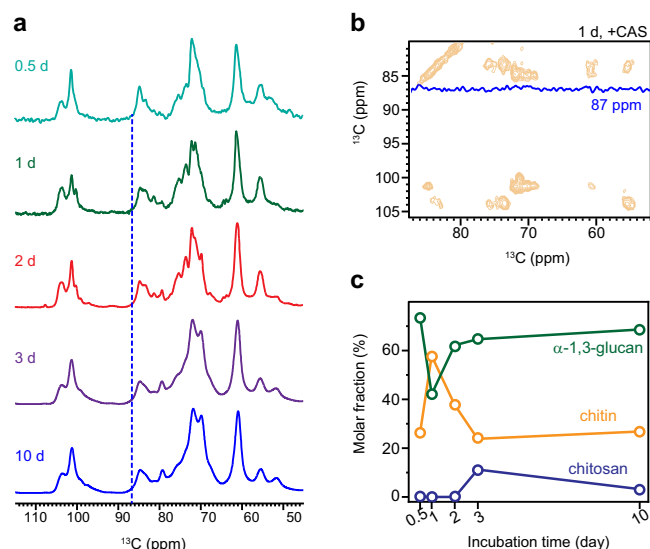
Fig. 3 | Evolution of polysaccharide composition during caspofungin treatment. a 1D CP spectra of caspofungin-treated *A. fumigatus* samples prepared with varied duration of culture. Blue dashed line indicates the characteristic position for the carbon-3 of β-1,3-glucan. **b** 2D ^{13}C CORD spectra of one-day-old caspofungin-treated *A. fumigatus* confirming the absence of β-1,3-glucans. The 1D cross-section is extracted at 86.5 ppm, the characteristic chemical shift for carbon 3 of β-1,3-glucan. **c** Estimation of rigid polysaccharide fractions derived from spectral deconvolution.

caspofungin, while the branched β-1,3/1,6-glucan is part of the mobile fraction of the cell wall.

Caspofungin dramatically increased the amount of α-1,3-glucan, from 44% to 61% and from 4% to 33% in the rigid and mobile fractions, respectively (Fig. 1g and Supplementary Table 4). The accumulation of α-glucan compared to β-glucans was further validated using chemical assays (Fig. 2d and Supplementary Table 5). Apart from the major type of α-1,3-glucan (A[a]) primarily found in the rigid fraction, two other magnetically inequivalent forms (A[b] and A[c]) were observed in both the rigid (Fig. 1f) and mobile fractions (Fig. 2b) of the caspofungin-treated sample. These two new types of α-1,3-glucans have not been reported previously and their chemical identities were confirmed by their absence from an *A. fumigatus* mutant and other fungal species that lack α-1,3-glucan (Supplementary Fig. 4). The three types of α-1,3-glucans exhibited distinct C3 chemical shift, ranging from 85 ppm for type-a to 79-81 ppm for types-b and c. Since C3 denotes the carbon position of the glycosidic linkage in this polysaccharide, the observed differences imply conformational alterations reflected in changes concerning the orientations of the glycosidic bonds and the adjacent sugar residues along the polymer. While the type-b and c forms exhibited very weak signals in the apo sample, they showed strong peaks in the *A. fumigatus* cell walls after caspofungin treatment (Supplementary Fig. 5). Thus, α-1,3-glucan simultaneously increased its amount and altered its structure to compensate for the loss of β-1,3-glucan. *A. fumigatus* cultures treated with anidulafungin and micafungin displayed spectra resembling those of caspofungin-treated cell walls (Supplementary Fig. 6), indicating similar structural changes induced by these echinocandins.

Other mobile polysaccharides, primarily GAG and GM, were largely conserved as shown by their comparable chemical shift fingerprints (Supplementary Fig. 7). Caspofungin halved the GAG content but did not perturb the molecular composition of the three sugar residues (Gal*p*, GalN, and GalNAc) within this heteroglycan (Fig. 1g and Supplementary Table 3). Due to the cationic state of GalN (present as GalNH$_3^+$) at cellular pH, the observed decrease in the GAG content will reduce the charge of the cell wall surface and affect the adhesive

property. Although the total amount of galactomannan (GM) remained unchanged, the proportion of Gal*f* decreased by one-third (Fig. 1g), indicative of shorter or fewer galactofuran sidechains in caspofungin-treated mycelia. The carbohydrate-to-protein/lipid ratio remained stable following treatment with caspofungin (Supplementary Figs. 8, 9 and Table 6), as well as anidulafungin and micafungin (Supplementary Fig. 6d). This indicates that the overall quantity of structural polysaccharides remained effectively preserved after exposure to echinocandins. Fluctuations in lipid and protein content were observed during shorter incubation periods (Supplementary Fig. 10), likely originating from a combination of extracellular and intracellular sources, including plasma membranes (Supplementary Fig. 11).

The evolving biopolymer composition over time was assessed by analyzing spectra of younger cultures. No resolvable signal for β-glucan in the rigid phase could be detected in *A. fumigatus* samples cultured between 0.5–10 days (Fig. 3a, b). Spectral deconvolution and subsequent analysis of peak area have shown that chitin emerged as the predominant fraction, constituting 60% of intact cell wall domains after 1 day of caspofungin exposure, reinforcing the cell wall for survival (Fig. 3c and Supplementary Fig. 12). However, its proportion subsequently declined rapidly to one-fifth of the rigid molecules after 3 days, while its acetylated form, chitosan, concurrently increased to 10%. The fluctuations of chitin consistently opposed those of α-1,3-glucans, suggesting their shared roles in maintaining cell wall structures.

Reduced water retention and polymer dynamics

A key finding is that caspofungin treatment leads to a reduction in the water accessibility of *A. fumigatus* cell walls, which was marked by the decline of intensities in 2D hydration maps (Fig. 4a). Such intensities reflect the capabilities of polymers to retain water molecules around various carbon sites (Supplementary Table 7). Upon caspofungin treatment, the relative intensities of α-glucan, chitin, and β-1,3-glucan in cell walls of 3-day-old cultures dropped by 27%, 39%, and 46%, respectively (Fig. 4b). This decrease in water retention and increase in hydrophobicity should contribute to the reduction in cell wall permeability.

The dynamical heterogeneity of cell wall polysaccharides was examined using ^{13}C spin-lattice (T_1) relaxation measurements, carried out in a pseudo-3D format to enhance spectral resolution (Supplementary Fig. 13). Within each sample, β-1,3-glucans showed high mobility on the nanosecond timescale, with relatively short ^{13}C-T_1 time constants of 1–3 s (Fig. 4c and Supplementary Table 8). Chitin, the major form of α-1,3-glucan (A[a]), and β-1,4-linked glucose units exhibited longer ^{13}C-T_1 values of 3-8 s. The stiffness of chitin and α-1,3-glucan is justified by their close association at the mechanical center, but the long T_1 values of β-1,4-linked glucose units, typically identified in the mix-linked β-1,3/1,4-glucan, are unexpected[26]. These β-1,3/1,4-glucans constitute minor segments that are occasionally covalently connected to the major β-1,3/1,6-glucan domains[30]. The data suggest that β-1,3/1,4-glucan is intrinsically inflexible, either achieved by maintaining physical separation from the bulk domain of mobile β-glucans or due to spatial constraints imposed by packing interactions with rigid molecules like chitin or α-glucan.

Caspofungin reshapes the dynamical landscape of the mechanical core in *A. fumigatus* cell walls. After treatment, the residual β-1,3-glucan (which transforms into highly branched β-1,3/1,6-glucan) was rigidified, with its average ^{13}C-T_1 increased apparently from 1.4-s to 2.0-s (Fig. 4c). Because most β-1,3-glucans residing in the soft matrix were eliminated due to drug inhibition, the remaining ones should primarily pack with rigid molecules. Caspofungin also rigidified chitin and increased its ^{13}C-T_1 from 2.6-s to 2.9-s. This could be attributed to the promoted aggregation of chitin chains in the absence of filling molecules (β-1,3-glucans). Conversely, β-1,4-linked glucose residues experienced an opposite shift, with almost halved ^{13}C-T_1 (from 5.5-s to 3.0-s).
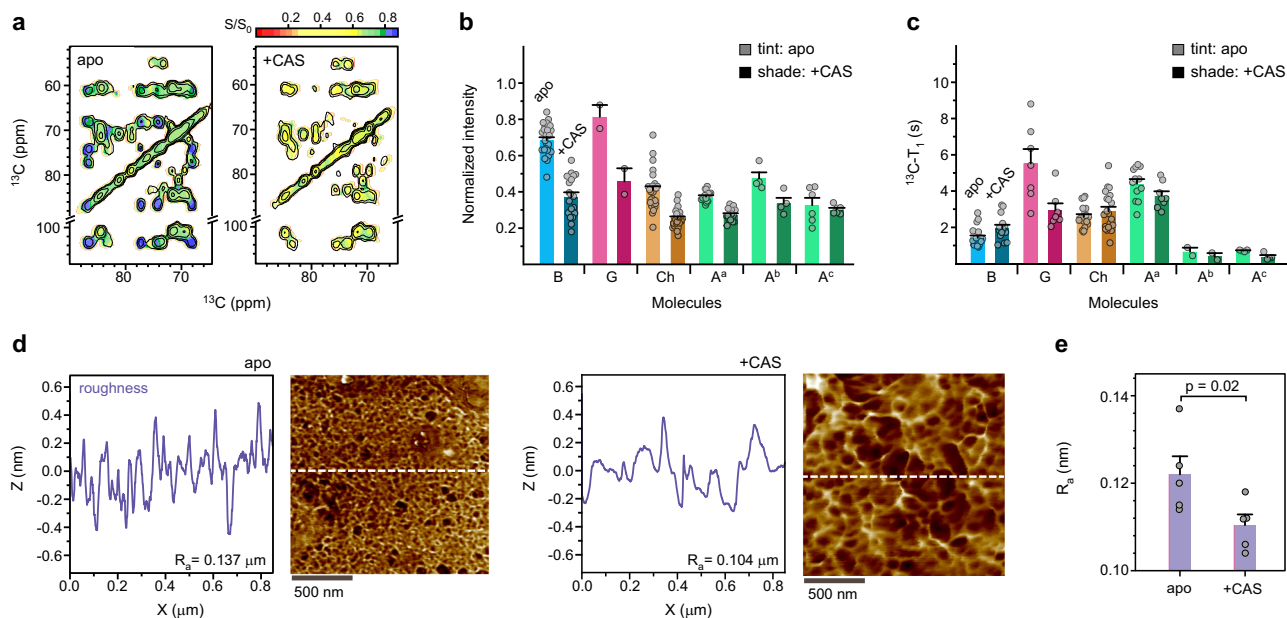
Fig. 4 | Effect of caspofungin on water accessibility, biopolymer rigidity, and surface roughness. a Hydration map of 3-day-old *A. fumigatus* without (top) and with (bottom) caspofungin treatment. This intensity map plotted the ratios (S/S₀) of peak intensities from the water-edited spectrum (S) detecting hydrated molecules, relative to those from the control spectrum (S₀) representing equilibrium conditions. **b** Relative intensities (S/S₀) of different carbon sites indicating the extent of water association of cell wall polysaccharides. Data are shown for apo and drug-treated samples: β-1,3-glucan (B; n = 25, 19), chitin (Ch; n = 25, 25), β-1,4-glucose units (G; n = 3, 3), and three subtypes of α-1,3-glucan (A^a, n = 16, 15; A^b, n = 4, 4; A^c, n = 6, 6). **c** ^{13}C-T$_1$ relaxation time constants for different carbon sites in 3-day-old *A. fumigatus* samples. Data are shown for carbohydrates in both apo and drug-treated samples: B (n = 20, 15), Ch (n = 20, 20), G (n = 7, 7), A^a, (n = 12, 8), A^b (n = 2, 2), and A^c (n = 6, 6). Data in panels **b** and **c** are presented as mean ± s.e., with data points superimposed on the bar diagram. **d** Lateral surface roughness profiles and corresponding AFM images of 3-day-old *A. fumigatus* without (apo, left) and with (+CAS, right) caspofungin exposure, showing difference in the average roughness (R$_a$). The white dashed lines denote the locations from which representative roughness profiles are derived. **e** Surface roughness determined by analyzing the lateral roughness profiles from five AFM images for both apo and drug-treated samples. Data are mean ± s.e. with n = 5 for apo and caspofungin-treated samples. The statistically significant differences (α = 0.02) were identified by unpaired Student *t*-test. Source data are provided as a Source Data file.

The removal of β-1,3-glucans has significantly impacted the stability of β-1,3/1,4-glucans, probably because these two polysaccharides were covalently linked to each other[30,31]. Similarly, the major form of α-1,3-glucan became moderately more dynamic, and the two minor forms are inherently dynamic, which should help to partially fulfill the diverse roles of the now-removed β-1,3-glucan. These two newly identified forms of α-1,3-glucans also displayed a distinct double-exponential feature (Supplementary Fig. 14 and Table 9), revealing their distribution across dynamically distinct regions.

While NMR uncovers dynamics and hydration at the molecular level, AFM provides direct measurement of cell wall surface topography and mechanical properties. Recent studies on *A. nidulans* have used AFM and subresolution imaging methods to determine the elastic modulus and its spatial gradient within the hyphae[32–34]. We analyzed the cellular-level surface roughness of 3-day-old *A. fumigatus* cultures using AFM (Fig. 4d) and observed a decrease in the lateral roughness in the drug-treated sample (Fig. 4e), indicating a smoothing effect of the fungal cell surface by caspofungin treatment.

Rearrangement of the macromolecular network

Fungal cell walls undergo significant spatial rearrangement in response to caspofungin. Assessment of the nanoscale assembly of macromolecules is enabled by the DNP technique, which relies on electron polarization to provide a 17-22-fold enhancement on the NMR sensitivity of two 3-day-old *A. fumigatus* samples (Fig. 5a)[35–37]. This enhancement results in a shortened experimental duration by 290 to 480 times. The cryogenic temperature required for DNP measurements has broadened the NMR linewidth and abolished the signals of highly disordered molecules such as GM and GAG, but the resolution remains adequate for resolving the diverse carbon and nitrogen sites

of major polysaccharides and visualizing their sparsely populated packing interfaces (Supplementary Fig. 15).

Caspofungin-treated samples showed unambiguous cross-peaks between the nitrogen of chitosan amine group (CsN) and the carbons of chitin and α-glucan (Fig. 5b), providing clear evidence of the nanoscale coexistence of these biomolecules. Notably, the amide nitrogen of chitin correlates predominantly with the carbons of α-1,3-glucan, forming a physically associated complex. This structural concept is further supported by the numerous ^{13}C-^{13}C cross-peaks between these two polysaccharides (Fig. 5c). In addition, four major forms of N-acetylglucosamine (GlcNAc) units were identified. These units engage in hydrogen-bonding to create crystalline microfibrils[38], and inter-form cross-peaks can be detected between the carbonyls (ChCO-CO') and between the methyl groups (ChMe-Me') of different conformers. These cross peaks represent physical contacts of two molecules occurring on the sub-nanometer length scale.

A statistical summary of 114 intermolecular cross peaks revealed the elimination of intermolecular contacts involving β-1,3-glucans, which is an expected outcome due to the depletion of this polysaccharide by caspofungin (Fig. 5d and Supplementary Fig. 16). In contrast, drug treatment promoted the extensive associations between chitin and α-1,3-glucan, thereby stabilizing the polymer complexes formed by these two macromolecules. The elevated levels of chitin and α-1,3-glucan in the caspofungin-treated sample may have additionally played a role in facilitating the detection of their physical contact. Chitosan was found to be anchored to this chitin-α-1,3-glucan core, and caspofungin treatment has strengthened this packing interaction. Chitosan could potentially exist as a constituent of chitin-chitosan copolymers that are sometimes referred to as partially
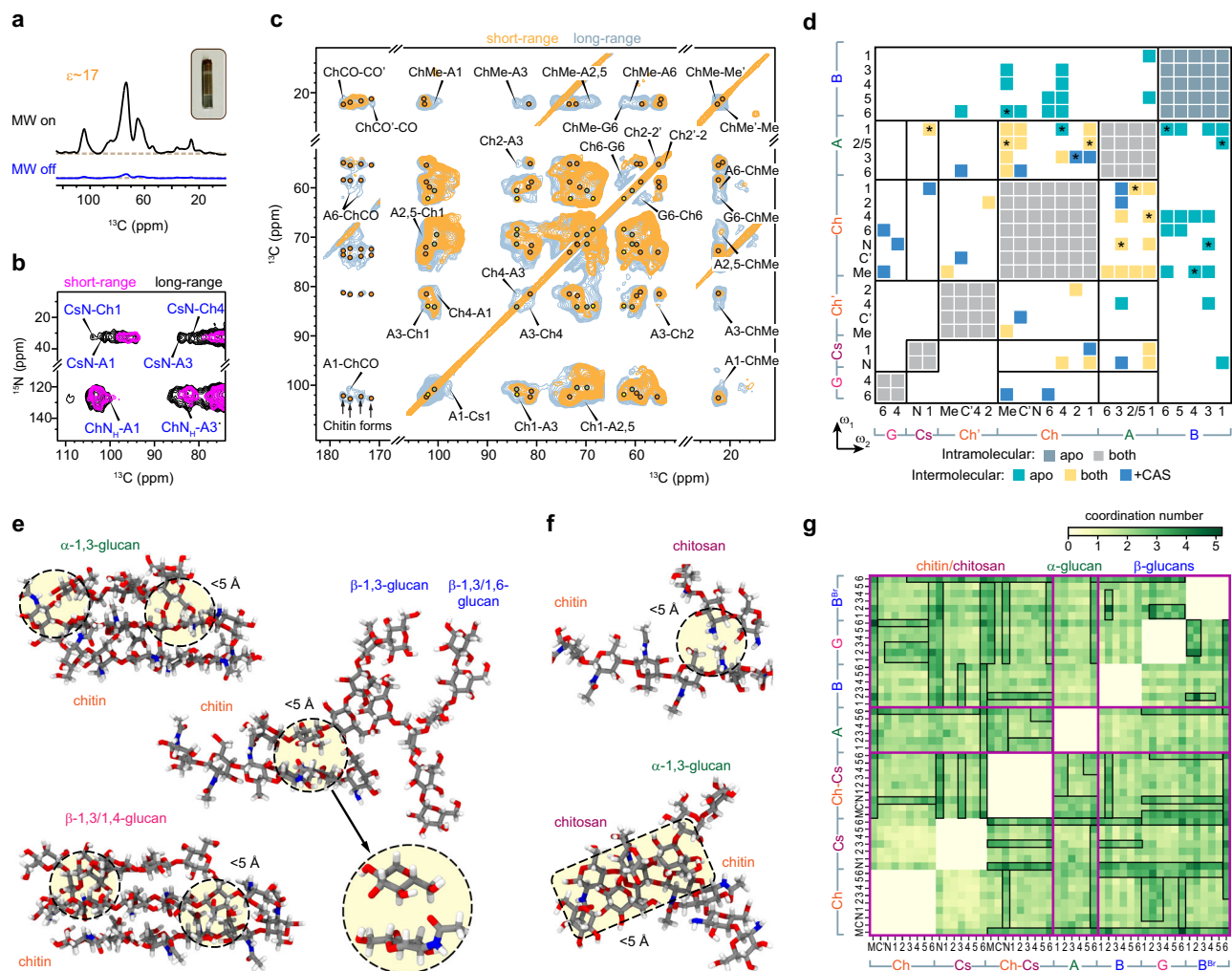
Fig. 5 | Intermolecular contacts in 3-day-old apo and caspofungin-treated *A. fumigatus*. **a** DNP enhances NMR sensitivity of the caspofungin-treated 3-day-old sample by 17-fold when microwave (MW) is activated. Inset shows the DNP sample with 30 mg hydrated mycelial material enclosed in a 3.2-mm sapphire rotor. Dash lines mark the baseline of the spectra. **b** DNP 2D ^{15}N-^{13}C correlation spectra of caspofungin-treated sample. Interactions happen between the ^{15}N-site of the chitin amide (ChN$_H$) or chitosan amine (CsN) and the carbons of polysaccharides. For example, CsN-A1 represents the cross peak between chitosan nitrogen with α−1,3-glucan carbon 1. **c** DNP 2D ^{13}C-^{13}C correlation spectra of caspofungin-treated sample. Most interactions happen between α-glucan and chitin. The carbonyl region showed four types of chitin signals. **d** Site-specific summary of inter-molecular cross peaks identified among different polysaccharides. Diagonal regions exhibit intramolecular cross peaks. Off-diagonal regions show inter-molecular interactions happening only in the apo sample (green), only in the drug-treated sample (blue), or in both samples (yellow). Strong intermolecular interactions from short-mixing spectra are marked with asterisks. The plot can be asymmetric relative to the diagonal due to the directionality of polarization transfer, e.g., Ch1-A3 differs from A3-Ch1. The left and bottom axes indicate the carbohydrate carbon numbers observed in indirect (ω_1) and direct (ω_2) spectral dimensions. Representative short-range interactions observed during 1 μs all-atom MD are shown between **e**, chitin, and glucans, and **f**, chitosan, and other polymers. Atoms in gray, red, blue, and white represent carbon, oxygen, nitrogen, and hydrogen, respectively. Packing interactions within 5 Å are highlighted. **g** Contact map of intermolecular interactions within 5 Å identified in MD models. The coor-dination number (see Methods) represents the number of contacts between two carbon sites of different polysaccharides. Magenta lines separate the sections of chitin/chitosan (Ch: chitin; Cs: chitosan; Ch-Cs: chitin-chitosan copolymer), α−1,3-glucan (A), and β-glucans (B: linear β−1,3-glucan; G: β−1,3/1,4-glucan; B^{Br}: β−1,3/1,6-glucan). Carbon and nitrogen numbers are provided on both axes (M: Me or methyl; C' carbonyl). Regions boxed in black highlight extensive interactions.

deacetylated chitin, or as fully deacetylated chains that are physically deposited onto the surface of chitin crystallites. Interestingly, β-1,4-linked glucose residues also showed several cross peaks with chitin. This suggests that β-1,3/1,4-glucan is trapped by chitin microfibrils, which explains the distinctive rigidity of this linear polymer as shown in Fig. 4c. Therefore, in the absence of the bridging molecule β-1,3-glucan, the stability of the *A. fumigatus* cell wall is sustained through many inter-allomorph interactions within chitin crystallites and inter-molecular associations involving chitin, α-1,3-glucans, chitosan, and β-1,3/1,4-glucan, collectively ensuring the maintenance of structural integrity.

Despite the potential involvement of protein and lipid in the cell wall architecture, no observable interactions were detected between these non-carbohydrate components and the cell wall poly-saccharides (Supplementary Fig. 17). This is likely due to the restricted physical interactions between these polymers. Alter-natively, the disorder nature of protein-carbohydrate complexes may result in signal broadening and rendering them undetectable at the cryogenic temperature of DNP. Nonetheless, some proteins and lipids still exhibit observable signals under these conditions. Recent chemical and NMR analyses have reported covalent connections between structural proteins and GM/GAG through unusual alkali-resistant linkers that incorporate hydrophobic amino acid residues such as valines[29]. This structural pattern remains unaffected in the caspofungin-treated cell wall, as evident from the consistent signals of valine and other amino acids in the rigid phase of the *A. fumigatus*

samples. It can be inferred that lipids and proteins have limited contact with cell wall polysaccharides, primarily associated with GM and GAG in the surface layer.

Microsecond-long all-atom molecular dynamics (MD) simulations have been employed to quantify intermolecular interactions and visualize polysaccharide packing interfaces in cell walls[39,40]. The solvated molecular system includes 14 polysaccharides, with two copies of each linear polysaccharides (chitin, chitosan, chitin-chitosan copolymer, α-1,3-glucan, β-1,3-glucan, and β-1,3/1,4-glucan) and the branched polymer β-1,3/1,6-glucan (Supplementary Fig. 18 and Movie 1). From microsecond-long unbiased MD trajectory, we systematically scanned over different cutoff distances to locate the best-fit trajectory, considering both short-range interactions (<7 Å) and long-range interactions (7-10 Å) based on the experimental observations provided by ssNMR. Chitin is physically aggregated with both α-1,3-glucan and the linear terminal chain of β-1,3/1,4-glucan (Fig. 5e and Supplementary Movie 2). The intermolecular distances are typically within 5.0 Å in the molecular trajectories, which rationalizes the strong cross-peaks observed among these polysaccharides in caspofungin-treated cell walls. Chitin also exhibited close-range interactions with both linear β-1,3-glucan and branched β-1,3/1,6-glucan; however, these molecules tend to be dispersed in space (Fig. 5e and Supplementary Movie 3). Chitin's association with chitosan was stable, with nitrogen-carbon/nitrogen distances of less than 5.0 Å (Fig. 5f and Supplementary Movie 4), highlighting the importance of hydrogen bonds involving nitrogen sites in chitin amide and chitosan amine. Short-range interactions were also observed between chitin-chitosan copolymers and α-1,3-glucans (Fig. 5f). Two chitin polymers also tend to exist as a stacked assembly (Supplementary Movie 5), which can serve as the platform to accommodate external molecules, such as α-1,3-glucan and β-1,3/1,4-glucan as shown in Fig. 5e. These simulation results explained the origin of NMR cross peaks happening between the chitosan introduced by caspofungin treatment and the stiff scaffold of chitin and α-glucan in the cell wall.

The interatomic contact map (Fig. 5g) allows us to visualize extensive short-range interactions (within 5 Å) between the chitin methyl group and the pyranose rings of both α-1,3- and β-glucans. The amine nitrogen of chitosan also played a major role in interacting with all three types of β-glucans. α-1,3-glucan is capable of interacting with both chitin and chitosan, utilizing its carbon-6 that extends outside the pyranose ring. Alternatively, all carbon sites of α-1,3-glucan predominantly interacted with the chitin-chitosan copolymer, a component that is possibly present only in the caspofungin-treated *A. fumigatus* cells. Therefore, the NMR-observed strong cross-peaks between α-1,3-glucan and chitin/chitosan after the depletion of β-1,3-glucan by caspofungin were not surprising. These unbiased all-atom MD models provided detailed structural insights into the pairwise interactions between different functional groups present in fungal polysaccharides.

Discussion

The fungal cell wall is an elastic entity that withstands hydrostatic turgor pressure, with microfibrillar components restricting stretching and matrix components countering compression[41]. Most polymers are interconnected by covalent linkages and held together by hydrogen bonds rather than as separate components[42]. Previous chemical and imaging studies and recent NMR data showed that the *A. fumigatus* mycelial cell wall comprises a mobile domain primarily composed of GAG, GM, and associated proteins, and an inner layer consisting of a β-glucan network that encompasses the hydrophobic and rigid junctions formed by physically packed chitin and α-glucans (Fig. 6a)[27,29]. At the same time, β-1,3-glucan also covalently crosslinks chitin and GM together, as revealed by chemical analysis[43]. Our findings have further reshaped our perception of the response of fungal cell walls to echinocandins (Fig. 6b).

First, a prominent alteration observed was the modification of the two amino-sugar polymers. The elevated level of chitin, which is a classical compensatory response for *A. fumigatus* to caspofungin and other cell wall stresses[44,45], was also shown in this study. It explains why chitin synthase mutants are more sensitive to caspofungin[46,47] and why combining Nikkomycin Z, a chitin synthase inhibitor, with caspofungin synergistically enhances the efficacy of caspofungin[48,49]. The enhanced chitin biosynthesis reinforces the rigidity of the cell wall while maintaining the polymorphic nature of the chitin structure and its association with other forms. However, an apparition of the high amount of chitosan was unexpected. The septuple chitin deacetylase mutant of *A. fumigatus* is not more sensitive to caspofungin[50], which would suggest that the chitosan likely does not play a significant role in maintaining the cell wall structure. Yet, recent data from *Aspergillus* species is illuminating the connection of chitosan with external stressors, including hypersaline conditions, as reported recently[51], and caspofungin exposure, as demonstrated here.

Second, the unexpected emergence of two novel allomorphs of α-1,3-glucans exhibiting a wide distribution within both rigid and mobile phases was noteworthy. While similar conformational changes have been documented in plant polysaccharides like xylan and homogalacturonan due to interactions with other polysaccharides or divalent cations[52–54], such phenomena have not been observed before in fungi. The stability of drug-treated cell walls is upheld by numerous physical interactions involving different chitin allomorphs and the interactions between chitin and α-1,3-glucans, which constrain molecular movements and restrict water accessibility within the cell wall. The increased resistance of the triple α-1,3-glucan synthase mutant to caspofungin compared to its parental strain[55] also suggests that the modification of α-1,3-glucan by caspofungin not only plays a structural role in cell wall maintenance but also regulates caspofungin penetration into fungal cells. This is further corroborated by previous studies which have frequently observed α-1,3-glucan to be predominantly located externally in *A. fumigatus*[56,57].

Third, under the experimental conditions tested which did not remove the entire cell wall β-glucan, the rigid and linear β-1,3-glucan almost vanishes, resulting in the subsequent removal of the covalently linked polysaccharide cores, such as (chitin-)β-1,3-glucan-GM and β-1,3-glucan-β-1,3/1,4-glucan, which are commonly found in untreated cells[43]. The remaining β-glucan predominantly exists within the mobile matrix and has undergone restructuring characterized by elevated β-1,6-branching, indicating that the extracellular remodeling process, controlled by members of the glycoside hydrolase GH-72 family[58], remained unaltered. The β-1,3/1,4-glucan linear domains became physically associated with chitin. Interestingly, the *tft1Δ* mutant lacking β-1,3/1,4-glucan is slightly more sensitive to caspofungin[31].

Fourth, a decrease in exopolysaccharide GAG content was noticed in caspofungin-treated cell walls, resulting in nearly equal proportions of GM and GAG on the cell wall surface. However, the impact of GAG on caspofungin susceptibility has been shown in the past to be minimum since mutants entirely lacking GAG or with increased GAG levels showed caspofungin susceptibility comparable to their parental strain[59,60]. GM also exhibits reduced content of Gal*f* sidechains in mycelia treated with the drug. Analysis of these galactose-based polysaccharides revealed altered galactose metabolism, likely as a compensatory mechanism for supporting cell wall integrity.

As β-glucan has been recognized as a key polysaccharide involved in covalently linking various components[61], the success of the cell walls devoid of most β-1,3-glucans holds two significant implications. First, it suggests that other polysaccharides can substitute for the structural role of β-1,3-glucan, enabling the survival of those fungi with highly intricate cell walls. Second, it emphasizes the importance of packing interactions and physical properties in stabilizing the biopolymer assembly and supporting the cell wall's function. The compromised water retention in the treated caspofungin due to the loss of β-glucan
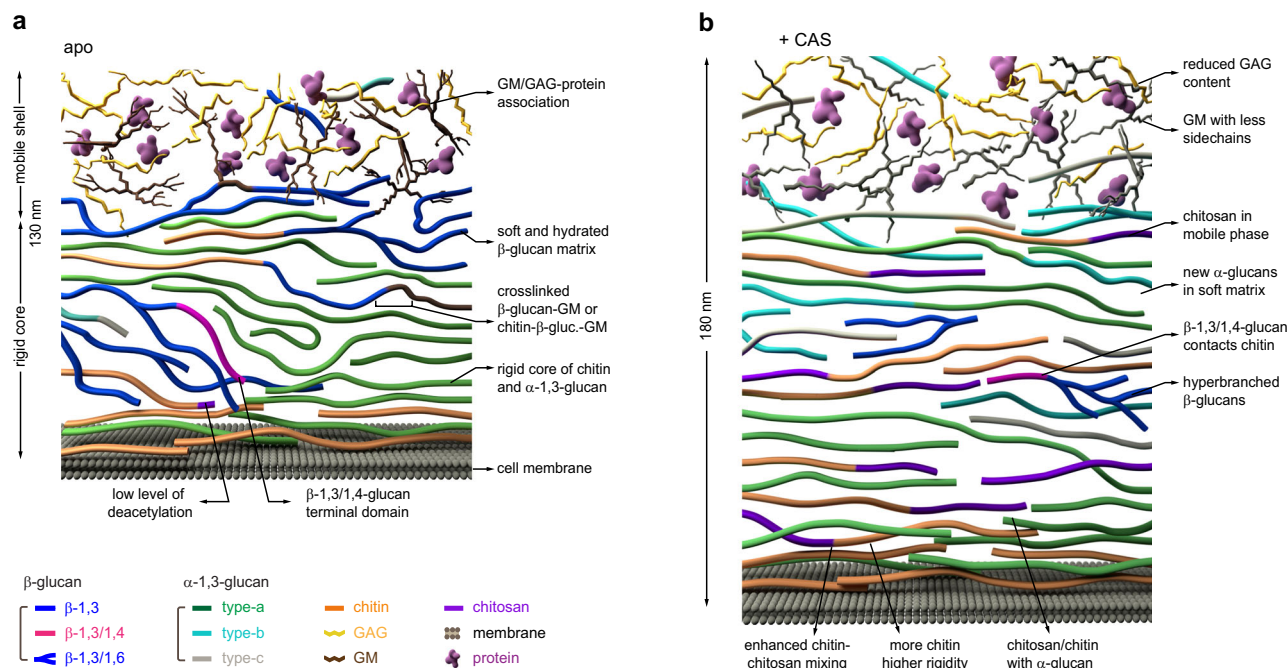
Fig. 6 | Schematic illustration of cell wall polysaccharide reorganization induced by caspofungin treatment. The illustration integrates NMR observations with the biochemical understanding of *A. fumigatus* cell walls. **a** Organization of cell wall polysaccharides in untreated 3-day-old *A. fumigatus* mycelial cell walls. The eight molecules shown in the figure include chitin (orange), α−1,3-glucan (green for type-a, cyan for type-b, and grey for type-c), β−1,3-glucan (blue, linear), β−1,3/1,6-glucan (blue, branched), β−1,3/1,4-glucan (magenta), chitosan (purple strands), GAG (yellow), GM (brown), cell membranes (dark grey), and proteins (purple particles). **b** Following caspofungin treatment, the amount of β−1,3-glucan is substantially reduced while the content of chitin, chitosan, and the two minor forms of α−1,3-glucans increased. The physical contacts among the remaining biopolymers also increased. These illustrative figures are constructed based on previous models[41,104] built on biochemical and imaging studies, and with new insights from current NMR analysis regarding molecular composition and intermolecular contacts. The sizes and orientations of the polymers depicted within the cell wall are hypothetical.

is key to maintaining water association within the cell wall. Third, the continuous and dynamic alterations in the concentration and composition of cell wall polymers induced by caspofungin, as shown by ssNMR data, are more rapid and complex than anticipated. Finally, these analyses also showed the importance of cell wall rigidity, and permeability in the drug influx or efflux.

Mutations in the *fks1* genes preventing the binding of echinocandins to the catalytic subunit FKS1 of β-1,3-glucan synthase[62,63] have been identified as responsible for the drug's limited efficacy. However, the survival of *A. fumigatus* during caspofungin treatment is largely FKS1-independent and arises from its tolerance to the drug, influenced by complex cellular and genetic interactions[64–66]. This tolerance includes well-documented phenomena such as the paradoxical effect, involving stress response pathways like Hsp90, calcineurin, and MAP kinases, and several transcription factors[64,65]. Twenty-one genes have been implicated in contributing to paradoxical growth[67]. Induction of reactive oxygen species (ROS) can also promote antifungal drug tolerance and the evolution of drug resistance[62]. Remodeling of the cell wall structure by drugs associated with the heterogeneity of fungal cell biology within a colony also significantly influences the subsequent penetration of cell wall-targeted drugs and the tolerance to these drugs[68].

Another important aspect to be emphasized in future antifungal studies is the modification of the cell wall permeability to the drug since remodeled cell wall structure can hinder the subsequent penetration of cell wall-targeted drugs[68]. While it is anticipated that cell wall modifications will vary depending on the drug utilized, the current findings have advanced our comprehension of cell wall structural integrity and have suggested promising avenues for improving antifungal therapies using cell-wall-targeting drugs. New drug combinations may emerge utilizing rezafungin[69], a new echinocandin,

manogepix, which targets GPI-anchored proteins controlling native polysaccharide modifications[70], and nanobodies[71] targeting chitin synthase, as no efficient anti-chitin synthase drug besides nikkomycin, which has not been used clinically, have been identified to date. This study has shown that the biophysical methodology holds the potential for thoroughly elucidating the restructuring impacts of diverse antifungal compounds, including both cell-wall targeting agents and those that do not specifically focus on polysaccharides, on cell wall structures during the adaptive survival of human fungal pathogens.

Methods

Preparation of ¹³C, ¹⁵N-fungal materials

A. fumigatus (strain RL 578) was grown in Yeast Extract Peptone Dextrose (YPD) for seven days at 30 °C. Liquid cultures were prepared using a modified minimum medium containing 10.0 g/L of ¹³C-glucose and 6.0 g/L of ¹⁵N-sodium nitrate for uniformly labeling the fungal material[72]. The medium was adjusted to pH 6.5. Two batches of *A. fumigatus* cultures were prepared in parallel, and the mycelium was recovered after 3 days of growth at a time when both apo and treated mycelia were in a linear phase of growth, thus excluding cell wall modifications attributed to autolysis during the stationary or declining phase of the fungus. The concentration of caspofungin drug used was 2.5 μg/mL, estimated as MIC 50 (inhibiting 50 % of the mycelial growth). *A. fumigatus* was grown in 100 mL liquid medium in 250 mL Erlenmeyer flasks in a shaking incubator (210 rpm) at 30 °C. The mycelia were collected by centrifugation at 7000 g for 20 min. The harvested pellets were then washed thoroughly using 10 mM phosphate buffer (PBS, pH 7.4). For each sample, approximately 100 mg of the whole-cell material was packed into a 4-mm magic-angle spinning (MAS) rotor for ssNMR characterization. Another 30 mg of material was packed into a 3.2-mm sapphire rotor for DNP experiments.

The native hydration level of the fungal cell was fully retained. Four additional samples were prepared under identical conditions and caspofungin concentration, with variations in culture duration (0.5 d, 1 d, 2 d, and 10 d) to understand the changes in polysaccharide composition. Additionally, two more batches of samples were prepared using the same protocol for 3-day-old cultures, but this time treated with micafungin and anidulafungin, each at a concentration of 2.5 μg/mL. In addition, *A. sydowii* was grown in minimum media with ^{15}N-ammonium sulfate for 7 days at 28 °C, and *C. albicans* was grown in yeast nitrogen-based (YNB) without amino acids and ammonium sulfate with ^{15}N-ammonium sulfate for 3 days at 30 °C. ^{13}C-glucose was used for both cultures as the carbon source.

TEM imaging

The harvested *A. fumigatus* mycelial cultures were fixed with 2.5% (vol/vol) glutaraldehyde and 2% (wt/vol) paraformaldehyde in 0.1 M PBS buffer (pH 7.4). The suspensions were centrifuged and embedded in 3% agarose gel. Subsequently, the samples were rinsed with 0.1 M PBS (pH 7.4), 0.05 M glycine, and then post-fixed with 2% osmium tetroxide (OsO$_4$). The samples were rinsed thrice using deionized water. Acetone (50%, 70%, 80%, 90%, and 100%) and propylene oxide were used to dehydrate the samples in two 15 minutes cycles. Finally, a series of propylene oxide: Epon was used for infiltration. Ultrathin sections of the resulting samples were taken for TEM assessments. To increase the contrast during imaging, 1% uranyl acetate *En Bloc* staining was used. In total, ten samples were analyzed, comprising both untreated and caspofungin-treated *A. fumigatus* samples collected at five different culture durations of 0.5 d, 1 d, 2 d, 3 d, and 10 d. All images were taken on perpendicular cross-sections of hyphae using a JEOL JEM-1400 electron microscope.

AFM analysis

Three-day-old untreated and caspofungin-treated *A. fumigatus* were used for AFM imaging in air. A single layer of cells was subjected on a glass slide and dried at room temperature. We employed the Bruker FastScan AFM system using ScanAsyst™ imaging mode and SCANASYST-AIR AFM probes (Bruker). All AFM images were taken under the same imaging settings: scan size 1 μm, samples/line 512, scan rate 1 Hz, with a nominal spring constant of 0.4 N/m. For each sample, imaging was performed with at least three independently prepared samples. The average roughness (Ra) of the lateral surface profile was determined from five representative images for each sample using Gwyddion software and a *t*-test assuming unequal variance was performed.

Cell wall fractionation and carbohydrate analysis

For carbohydrate analysis, mycelia were disrupted with 1 mm glass beads in 0.2 M Tris-HCl buffer, pH 8.0 with a fast-prep cell disruptor (MP-Bio). Crude cell wall fraction was collected by centrifugation ($4500 \times g$, 10 min), washed three times with distilled water, and then fractionated into alkali-insoluble and alkali-soluble portions[30,73]. Hexose and hexosamine were quantified by colorimetric and chromatographic assays[30,73]. Neutral monosaccharides were analyzed by gas-liquid chromatography (GC) as alditol acetates obtained after hydrolysis (4 N trifluoroacetic acid, 100 °C, 4 h). Derivatized monosaccharides were separated and quantified on a DB5 capillary column (25 m x 0.32 mm, SGE) using a Perichrom GC apparatus (carrier gas, 0.7 bar helium; temperature program, 120-180 °C at 2 °C/min and 180–240 °C at 4 °C/min). To quantify the content of hexosamine, cell wall fractions were hydrolyzed with 6 N HCl at 100 °C for 6 h and were analyzed by high-performance anion exchange chromatography (HPAEC) with a pulsed electrochemical detector and an anion exchange column (CarboPAC PA-1, 4.6 × 250 mm, Dionex) using 18 mM NaOH as mobile phase at a flow rate of 1 mL/min; glucosamine and galactosamine were used as standards.

To quantify β-1,3-glucan and α-1,3-glucan in the cell wall, the alkali-insoluble fraction and the water-soluble supernatant fraction were submitted to enzymatic digestions. Fractions (1 mg/mL) were incubated with recombinant β-1,3-glucanase (LamA from *Thermotoga neapolitana*) and the mutanase from *Trichoderma harzianum*, respectively, in 20 mM sodium acetate buffer (pH 5.5) at 37 °C for 24 h. The reducing sugar released after enzyme digestion were quantified by the 4-hydroxybenzhydrazide (PABA) assay. To quantify β-1,6-branching in β-1,3-glucan and β-1,3/1,4-glucan, the enzyme digests of different cell wall fractions were subjected to HPAEC using a CarboPAC PA-1 column (4.6 × 250 mm, Dionex) at a flow rate of 1 mL/min; eluent A was 50 mM NaOH, and eluent B was 0.5 M NaOAc in 50 mM NaOH. The elution gradient was: 0–2 min, isocratic 98% A:2% B; 2–15 min, linear gradient from 98% A:2% B to 65% A:35% B; 15–35 min, linear gradient from 65% A:35% B to 30% A:70% B, followed by 100% B for 3 min. Glycosidic linkages were investigated by methylation of cell wall fractions followed by GC-MS analysis[73,74]. The amount of cell wall galactomannan was estimated from the mannose and galactose content of the alkali-insoluble fraction.

SsNMR experiments for structural analysis

Most NMR experiments were conducted on a Bruker Avance 400 MHz (9.4 Tesla) spectrometer and an 800 MHz (18.8 Tesla) using 4-mm and 3.2-mm MAS HCN probes, respectively. Micafungin and anidulafungin-treated samples were analyzed using an 850 MHz NMR spectrometer. All experimental data, except those for MAS-DNP, were collected under 10–13.5 kHz MAS at 290 K. ^{13}C chemical shifts were externally referenced to the adamantane CH$_2$ peak at 38.48 ppm on the tetramethylsilane (TMS) scale. ^{15}N chemical shifts were referenced to the liquid ammonia scale either externally through the methionine amide resonance (127.88 ppm) of the model tri-peptide N-formyl-Met-Leu-Phe-OH or using the ratio of the gyromagnetic ratios of ^{15}N and ^{13}C[75]. Typical radiofrequency field strengths, unless specifically mentioned, were 80–100 kHz for ^{1}H decoupling, 62.5 kHz for ^{1}H hard pulses, 50–62.5 kHz for ^{13}C, and 41 kHz for ^{15}N. The experimental conditions were listed in Supplementary Table 10.

One-dimensional (1D) ^{13}C spectra were obtained using different polarization methods to selectively detect the rigid and mobile components of the fungal molecules. The rigid components were detected by 1D ^{13}C cross-polarization (CP) using 1-ms contact time. Quantitative detection and mobile components located inside the cell wall were measured by 1D ^{13}C direct polarization (DP) using short (2-s) and long (35-s) recycle delays, respectively. Spectral deconvolution was conducted on 1D ^{13}C CP spectra of caspofungin-treated *A. fumigatus* samples cultured for 0.5, 1, 2, 3, and 10 days. The parameter provided by the DMfit software[76] (version dmfit#20230120) is provided in Supplementary Table 11. 2D ^{13}C-^{13}C 53-ms CORD homonuclear correlation spectra were obtained to detect intramolecular cross-peaks and 2D ^{15}N-^{13}C N(CA)CX heteronuclear correlation spectra were obtained to detect amide signals of chitin[77]. To measure N(CA)CX, 0.6-ms ^{1}H-^{15}N CP, 5-ms ^{15}N-^{13}C CP contact times, and 100-ms DARR mixing time were used. The 2D DP refocused J-INADEQUATE spectra were obtained to detect mobile components with through bond connectivity. The assigned ^{13}C and ^{15}N signals were documented in Supplementary Table 12.

To determine the water accessibility of polysaccharides, water-edited 2D ^{13}C-^{13}C correlation spectra were obtained[78,79]. The experiment was initiated with ^{1}H excitation followed by a ^{1}H-T$_2$ filter of 1.2-ms × 2, which eliminated 97% of the polysaccharide signals but retained 80% of water magnetization. The water magnetization was then transferred to the polysaccharide using a 4-ms ^{1}H mixing period and then transferred to ^{13}C through a 1-ms ^{1}H-^{13}C CP for site-specific detection. A 50-ms DARR mixing period was used for both the water-edited spectrum and a control 2D spectrum showing the full intensity. The relative intensity ratio between the water-edited spectrum and the control spectrum was

quantified for all cell walls to reflect the relative extent of hydration (Supplementary Table 7). The intensities were pre-normalized by the number of scans of each spectrum. Hydration maps were generated using a python script integrated with nmrglue and matplotlib packages[80,81].

Polysaccharide dynamics were probed using ^{13}C spin-lattice (T_1) relaxation, which was examined using a series of 2D ^{13}C-^{13}C correlation spectra with different z-filter durations (0-s, 0.1−s, 1-s, 3-s, and 9-s)[82]. The absolute intensity of each peak was quantified and then normalized by the number of scans. Relaxation data were fit using a single exponential function to obtain ^{13}C-T_1 time constants (Supplementary Table 8). Some relaxation curves exhibited a distinct double-exponential feature, particularly for the two new types of α-1,3-glucans, and therefore were fit separately using double exponential functions (Supplementary Table 9).

MAS-DNP sample preparation and experiments
The stock solution containing 10 mM AMUPol was freshly prepared using a d_8-glycerol/D_2O/H_2O (60/30/10 Vol%) solvent mixture, typically named DNP-matrix[83]. Around 30 mg of ^{13}C,^{15}N-labeled mycelial cells were mixed with 50 μL of stock solution and gently ground using a mortar and pestle for 10-15 min, which allows radicals to penetrate the porous cell walls. The material was then transferred to a 3.2-mm sapphire rotor for the DNP measurement. All DNP experiments were performed on a 600 MHz/395 GHz 89 mm-bore MAS-DNP spectrometer equipped with a gyrotron microwave source[84]. All spectra were measured using a 3.2-mm HCN probe under 8 kHz MAS frequency at 92 K. The microwave power was set to 12 W at the probe base. The enhancement factor of NMR sensitivity with and without microwave irradiation ($\varepsilon_{on/off}$) was 17−32 for these samples. The buildup time varied between 5.2−13-s.

2D ^{13}C-^{13}C 100-ms PDSD were measured to detect intra-molecular correlations, followed by 20-ms PAR measurement to detect both intra- and inter-molecular correlations in carbohydrates of each cell wall[85]. The ^{13}C and ^1H irradiation frequencies were 56 kHz and 53 kHz during the PAR mixing. 2D ^{15}N-^{13}C N(CA)CX spectra were measured using the double-CP sequence[86], with 1.0 ms contact time for the ^1H-^{15}N CP and 4.0 ms for the ^{15}N-^{13}C CP. In these ^{15}N-^{13}C experiments, ^{13}C-^{13}C mixing was achieved using a PDSD period of either 0.1 s for detecting intramolecular cross peaks or 3.0 s for detecting both intra- and inter-molecular cross peaks. The resonance assignment under DNP condition was presented in Supplementary Fig. 15a−d, with the chemical shifts documented in Supplementary Table 13. The identified long-range intermolecular cross peaks were listed in Supplementary Table 14. Spectral asymmetry was noted for some cross peaks, attributed to differing protonation states and relaxation properties of the two carbon sites engaged in intermolecular correlation (Supplementary Fig. 19), a phenomenon previously noted in cell wall systems[87,88].

Construction of atomic models for MD simulation
We first assembled model α- and β-glucans using CHARMM-GUI Glycan Modeler[89,90]. The degree of polymerization (D.P.) of each polysaccharide was set to six monomers, which allowed us to keep the total system size of the whole system under 200,000 atoms as detailed later. Although the D.P. of the polysaccharide in the native fungal cell wall is significantly higher, the current atomistic model allows us to evaluate the structure-based polymer interactions. The CHARMM-GUI Glycan Modeler then assembled the short linear polysaccharides, α-1,3-glucan, β-1,3-glucan, and β-1,3/1,4-glucan as well as the branched β-1,3/1,6-glucan (Supplementary Fig. 18a). Similarly, short chitin polymers were generated using the plugin chitin_builder[91], within visual molecular dynamics (VMD 1.9.4a55)[92]. Chitin and chitosan are copolymers of 2-acetamido-2-deoxy-D-glucose (N-acetyl glucosamine, GlcNAc), and 2-amino-2-deoxy-D-glucose (glucosamine, GlcNH₂), connected by

β-1,4 glycoside linkages[93]. Chitin and chitosan might exist as a copolymer, with a variable degree of N-acetylation. In addition to the copolymer in our molecular system, we created separate polymers for chitin and chitosan to accurately track the individual interactions specific to each of the two polysaccharides. Since glucosamine in the existing CHARMM carbohydrate force field carries a charge[94,95], we introduced a patch to modify the topology and convert glucosamine into a monosaccharide unit of chitosan by deleting hydrogen and reparametrizing the charges. The final system has two copies of each polysaccharide, which were solvated in a box of water using the solvate plugin in VMD 1.9.4a55, with 5 mM of NaCl added to the hydrated neutralized model using the autoionize plugin to VMD 1.9.4a55[92]. The atomistic model consists of 120,972 atoms after adding solvent and ions (Supplementary Fig. 18b).

MD simulation and analysis of molecular trajectories
All-atom classical MD simulations for the models illustrated in Fig. 5e, f and Supplementary Fig. 18 were initially minimized using NAMD 2.14, to prepare for production simulations using the GPU resident integrator in NAMD 3.0a9. The simulation employed the CHARMM36 force fields for computing the interactions between carbohydrates[94,95], water[96], and ions[97]. Following CHARMM36 force field, we used a 12 Å cutoff and a force-switching function after 10 Å. Long-range electrostatics are treated using the particle mesh Ewald with a 1.2 Å grid spacing[98]. To enable a 2 fs timestep between force evaluations, covalent bonds involving hydrogen atoms were treated using the RATTLE algorithm[99]. The Langevin thermostat was set to maintain a temperature of 300 K using a 5 ps^{-1} damping coefficient[100]. A microsecond-long MD simulation was performed for an NPT ensemble, using a Langevin isotropic barostat that was set to maintain 1 atm pressure[101].

The simulation trajectory was analyzed using VMD 1.9.4a55, which was enabled with Python 3.10.12 and Numpy 1.24.2[102]. In-house scripts were prepared in Tcl 8.6 and Python 3.10.12 programming software to calculate and quantify the intermolecular interactions between polysaccharides using the coordination number collective variable[103]. The coordination number (C_{ij}) measures the pairwise contact between two atoms within a given polymer chain. This was implemented using a switching function defined as $C_{ij} = \sum_i \sum_{j \neq i} 1 - (|x_i - x_j|/d_o)^n / 1 - (|x_i - x_j|/d_o)^m$. Short- and long-range interactions were defined using the cutoff parameter, which used the switching distance to define an interatomic contact, for all $d \ll d_0$. Exponents n and m are set to 10 and 120, to steepen the switching profile. The equation for the coordination number is illustrated in Supplementary Fig. 18d for short-range and long-range cutoff 5 and 7 Å with the exponents $n = 10$ and m = 120. A contact map illustrating the polysaccharide interactions within 5 Å from each other was computed to probe the short-range interactions in the fungal cell wall (Fig. 5g). Time-course analysis from triplicate all-atom MD simulations for the sum of all intermolecular contacts between the polysaccharides within 5 Å is included as Supplementary Fig. 20. All system preparation, molecular simulation input, and analysis script are made publicly available on Zenodo.

Reporting summary
Further information on research design is available in the Nature Portfolio Reporting Summary linked to this article.

Data availability
All NMR spectra and biochemical data that support the findings of this study are provided in the article and Supplementary Information. The topspin NMR datasets of all ssNMR spectra collected on fungal cell walls are available in the public repository Zenodo under the DOI number: https://doi.org/10.5281/zenodo.12700137. Source data are provided with this paper.

Code availability

All MD input data, which includes topology, force field parameters and input scripts that support the findings of this research are publicly available via Zenodo under the DOI number https://doi.org/10.5281/zenodo.12700137.

References

1. Garcia-Vidal, C., Viasus, D. & Carratala, J. Pathogenesis of invasive fungal infections. *Curr. Opin. Infect. Dis.* **26**, 270–276 (2013).

2. Erwig, L. P. & Gow, N. A. R. Interactions of fungal pathogens with phagocytes. *Nat. Rev. Microbiol.* **14**, 163–176 (2016).

3. Denning, D. W. Global incidence and mortality of severe fungal disease. *Lancet Infect. Dis.* **24**, e428–e438 (2024).

4. Hoenigl, M. Invasive fungal disease complicating Coronavirus Disease 2019: When it rains, it spores. *Clin. Infect. Dis.* **73**, e1645–e1648 (2021).

5. Hoenigl, M. et al. COVID-19-associated fungal infections. *Nat. Microbiol.* **7**, 1127–1140 (2022).

6. Ghannoum, M. A. & Rice, L. B. Antifungal agents: mode of action, mechanisms of resistance, and correlation of these mechanisms with bacterial resistance. *Clin. Microbiol. Rev.* **12**, 501–517 (1999).

7. Verweij, P. E., Snelders, E., Kema, G. H. J., Mellado, E. & Melchers, W. J. G. Azole resistance in Aspergillus fumigatus: a side-effect of environmental fungicide use? *Lancet Infect. Dis.* **9**, 789–795 (2009).

8. Odds, F. C., Brown, A. J. P. & Gow, N. A. R. Antifungal agents: Mechanisms of action. *Trends Microbiol* **11**, 272–279 (2003).

9. Hasim, S. & Coleman, J. J. Targeting the fungal cell wall: current therapies and implications for development of alternative antifungal agents. *Future Med. Chem.* **11**, 869–883 (2019).

10. Perlin, D. S. Current perspectives on echinocandin class drugs. *Future Microbiol.* **6**, 441–457 (2011).

11. Chen, S. C. A., Slavin, M. A. & Sorrell, T. C. Echinocandin antifungal drugs in fungal infections. *Drugs* **71**, 11–41 (2011).

12. SC, D. & Stevens, D. A. Caspofungin. *Clin. Infect. Dis.* **36**, 1445–1457 (2003).

13. Hu, X. et al. Structural and mechanistic insights into fungal β-1,3-glucan synthase FKS1. *Nature* **616**, 190–198 (2023).

14. Reboli, A. C. et al. Anidulafungin versus fluconazole invasive candidiasis. *N. Engl. J. Med.* **356**, 2472–2482 (2007).

15. Pappas, P. G. et al. Micafungin versus caspofungin for treatment of candidemia and other forms of invasive candidiasis. *Clin. Infect. Dis.* **45**, 883–893 (2007).

16. Latgé, J. P. The pathobiology of Aspergillus fumigatus. *Trends Microbiol.* **9**, 382–389 (2001).

17. Latgé, J. P. Aspergillus fumigatus and aspergillosis. *Clin. Microbiol. Rev.* **12**, 310–350 (1999).

18. Bowman, J. C. et al. The antifungal echinocandin caspofungin acetate kills growing cells of Aspergillus fumigatus in vitro. *Antimicrob. Agents Chemother.* **46**, 3001–3012 (2002).

19. Hopke, A., Brown, A. J. P., Hall, R. A. & Wheeler, R. T. Dynamic fungal cell wall architecture in stress adaptation and immune evasion. *Trends Microbiol.* **26**, 284–295 (2018).

20. Garcia-Rubio, R., de Oliveira, H. C., Rivera, J. & Trevijano-Contador, N. The fungal cell wall: Candida, Cryptococcus, and Aspergillus species. *Front. Microbiol.* **10**, 2993 (2020).

21. Klis, F. M., Mol, P., Hellingwerf, K. & Brul, S. Dynamics of cell wall structure in Saccharomyces cerevisiae. *FEMS Microbiol. Rev.* **26**, 239–256 (2002).

22. Cowen, L. E. & Steinbach, W. J. Stress, drugs, and evolution: the role of cellular signaling in fungal drug resistance. *Eukaryot. Cell* **7**, 747–764 (2008).

23. Safeer, A. et al. Probing cell-surface interactions in fungal cell walls by high-resolution 1H-detected solid-state NMR Spectroscopy. *Chem. Eur. J.* **29**, e202202616 (2022).

24. Chrissian, C. et al. Solid-state NMR spectroscopy identifies three classes of lipids in Cryptococcus *neoformans* melanized cell walls whole fungal cells. *J. Biol. Chem.* **295**, 15083–15096 (2020).

25. Ghassemi, N. et al. Solid-state NMR investigations of extracellular matrixes and cell walls of algae, bacteria, fungi, and plants. *Chem. Rev.* **122**, 10036–10086 (2022).

26. Kang, X. et al. Molecular architecture of fungal cell walls revealed by solid-state NMR. *Nat. Commun.* **9**, 2747 (2018).

27. Latgé, J. P. & Wang, T. Modern biophysics redefines our understanding of fungal cell wall structure, complexity, and dynamics. *mBio* **13**, e0114522 (2022).

28. Lamon, G. et al. Solid-state NMR molecular snapshots of Aspergillus fumigatus cell wall architecture during a conidial morphotype transition. *Proc. Natl Acad. Sci. USA* **120**, e2212003120 (2023).

29. Chakraborty, A. et al. A molecular vision of fungal cell wall organization by functional genomics and solid-state NMR. *Nat. Commun.* **12**, 6346 (2021).

30. Fontaine, T. et al. Molecular organization of the alkali-insoluble fraction of *Aspergillus fumigatus* cell wall. *J. Biol. Chem.* **275**, 27594–27607 (2000).

31. Samar, D., Kieler, J. B. & Klutts, J. S. Identification and deletion of Tft1, a predicted glycosyltransferase necessary for cell wall β-1, 3; 1, 4-glucan synthesis in Aspergillus fumigatus. *PLoS One* **10**, e0117336 (2015).

32. Chevalier, L. et al. Cell wall dynamics stabilize tip growth in a filamentous fungus. *PloS Biol.* **21**, e3001981 (2023).

33. Davi, V. et al. Systematic mapping of cell wall mechanics in the regulation of cell morphogenesis. *Proc. Natl Acad. Sci. USA* **116**, 13833–13838 (2019).

34. Zhao, L. et al. Elastic properties of the cell wall of Aspergillus nidulans studied with atomic force microscopy. *Biotechnol. Prog.* **21**, 292–299 (2005).

35. Ni, Q. Z. et al. High frequency dynamic nuclear polarization. *Acc. Chem. Res.* **46**, 1933–1941 (2013).

36. Mentink-Vigier, F., Akbey, Ü., Oschkinat, H., Vega, S. & Feintuch, A. Theoretical aspects of magic angle spinning-dynamic nuclear polarization. *J. Magn. Reson.* **258**, 102–120 (2015).

37. Koers, E. J. et al. NMR-based structural biology enhanced by dynamic nuclear polarization at high magnetic field. *J. Biomol. NMR* **60**, 157–168 (2014).

38. Fernando, L. D. et al. Structural polymorphism of chitin and chitosan in fungal cell walls from solid-state NMR and principal component analysis. *Front. Mol. Biosci.* **8**, 727053 (2021).

39. Sarkar, D. et al. Diffusion in intact secondary cell wall models of plants at different equilibrium moisture content. *Cell Surf.* **9**, 100105 (2023).

40. Vermaas, J. V. et al. Mechanism of lignin inhibition of enzymatic biomass deconstruction. *Biotechnol. Biofuels Bioprod.* **8**, 217 (2015).

41. Gow N. A. R., Latge, J. P. & Munro, C. A. The fungal cell wall: structure, biosynthesis, and function. *Microbiol. Spectr.* **5**, FUNK-0035-2016 (2017).

42. Wessels, J. G. H. Developmental regulation of fungal cell wall formation. *Annu. Rev. Phytopathol.* **32**, 413–437 (1994).

43. Latgé, J. P. The cell wall: a carbohydrate armour for the fungal cell. *Mol. Microbiol.* **66**, 279–290 (2007).

44. Walker, L. A., Lee, K. K., Munro, C. A. & Gow, N. A. Caspofungin treatment of aspergillus fumigatus results in ChsG-dependent upregulation of Chitin synthesis and the formation of Chitin-rich microcolonies. *Antimicrob. Agents Chemother.* **59**, 5932–5941 (2015).

45. Wagner, A. S., Lumsdaine, S. W., Mangrum, M. M. & Reynolds, T. B. Caspofungin-induced β(1,3)-glucan exposure in Candida albicans is driven by increased chitin levels. *mBio* **14**, e0007423 (2023).

46. Jiménez-Ortigosa, C. et al. Chitin synthases with a myosin motor-like domain control the resistance of Aspergillus fumigatus to echinocandins. *Antimicrob. Agents Chemother.* **56**, 6121–6131 (2012).

47. Muszkieta, L. et al. Deciphering the role of the chitin synthase families 1 and 2 in the in vivo and in vitro growth of Aspergillus fumigatus by multiple gene targeting deletion. *Cell Microbiol.* **16**, 1784–1805 (2014).

48. Verwer, P. E., van Duijn, M. L., Tavakol, M., Bakker-Woudenberg, I. A. & van de Sande, W. W. Reshuffling of Aspergillus fumigatus cell wall components chitin and β-glucan under the influence of cas-pofungin or nikkomycin Z alone or in combination. *Antimicrob. Agents Chemother.* **56**, 1595–1598 (2012).

49. Ganesan, L. T., Manavathu, E. K., Cutright, J. L., Alangaden, G. J. & Chandrasekar, P. H. In-vitro activity of nikkomycin Z alone and in combination with polyenes, triazoles or echinocandins against Aspergillus fumigatus. *Clin. MIcrobiol. Infect.* **10**, 961–966 (2004).

50. Mouyna, I. et al. What are the functions of Chitin Deacetylases in Aspergillus fumigatus? *Front. Cell. Infect. Microbiol.* **10**, 28 (2020).

51. Fernando, L. D. et al. Structural adaptation of fungal cell wall in hypersaline environment. *Nat. Commun.* **14**, 7082 (2023).

52. Simmons, T. J. et al. Folding of xylan onto cellulose fibrils in plant cell walls revealed by solid-state NMR. *Nat. Commun.* **7**, 13902 (2016).

53. Kirui, A. et al. Carbohydrate-aromatic interface and molecular architecture of lignocellulose. *Nat. Commun.* **13**, 538 (2022).

54. Temple, H. et al. Golgi-localized putative S-adenosyl methionine transporters required for plant cell wall polysaccharide methylation. *Nat. Plants* **8**, 656–669 (2022).

55. Valsecchi, I. et al. The puzzling construction of the conidial outer layer of Aspergillus fumigatus. *Cell Microbiol* **21**, e12994 (2019).

56. Fontaine, T. et al. Cell wall alpha1-3glucans induce the aggregation of germinating conidia of Aspergillus fumigatus. *Fungal Genet. Biol.* **47**, 707–712 (2010).

57. Loussert, C. et al. In vivo biofilm composition of Aspergillus fumigatus. *Cell Microbiol* **12**, 405–410 (2010).

58. Mouyna, I. et al. Glycosylphosphatidylinositol-anchored gluca-nosyltransferases play an active role in the biosynthesis of the fungal cell wall. *J. Biol. Chem.* **275**, 14882–14889 (2000).

59. Gravelat, F. N. et al. Aspergillus galactosaminogalactan mediates adherence to host constituents and conceals hyphal β-glucan from the immune system. *PLOS Pathog.* **9**, e1003575 (2013).

60. Lamarre, C. et al. Galactofuranose attenuates cellular adhesion of Aspergillus fumigatus. *Cell Microbiol* **11**, 1612–1623 (2009).

61. Aimanianda, V. et al. The dual activity responsible for the elongation and branching of β-(1,3)-Glucan in the fungal cell wall. *mBio* **8**, 00619–00617 (2017).

62. Satish, S. et al. Stress-induced changes in the lipid microenvironment of β-(1, 3)-d-glucan synthase cause clinically important echinocandin resistance in Aspergillus fumigatus. *mBio* **10**, e00779–00719 (2019).

63. Jimenez-Ortigosa, C., Moore, C., Denning, D. W. & Perlin, D. S. Emergence of Echinocandin resistance due to a point mutation in the fks1 Gene of Aspergillus fumigatus in a patient with chronic pulmonary Aspergillosis. *Antimicrob. Agents Chemother.* **61**, e01277–01217 (2017).

64. Loiko, V. & Wagener, J. The paradoxical effect of echinocandins in Aspergillus fumigatus relies on recovery of the β-1, 3-glucan synthase Fks1. *Antimicrob. Agents Chemother.* **61**, e01690–01616 (2017).

65. Valero, C. et al. Caspofungin paradoxical effect is a Tolerant "Eagle Effect" in the filamentous fungal pathogen Aspergillus fumigatus. *mBio* **13**, e0044722 (2022).

66. Gonzalez-Jimenez, I., Perlin, D. S. & Shor, E. Reactive oxidant species induced by antifungal drugs: identity, origins, functions, and connection to stress-induced cell death. *Front. Cell. Infect. Microbiol.* **13**, 1276406 (2023).

67. Zhao, S. et al. Genomic and molecular identification of genes contributing to the Caspofungin Paradoxical effect in Aspergillus fumigatus. *Microbiol. Spectr.* **10**, 00519–00522 (2022).

68. Liu, Z. et al. Functional genomic and biochemical analysis reveals pleiotropic effect of Congo red on Aspergillus fumigatus. *mBio* **12**, e00863–00821 (2021).

69. Wiederhold, N. P., Locke, J. B., Daruwala, P. & Bartizal, K. Rezafungin (CD101) demonstrates potent in vitro activity against Aspergillus, including azole-resistant Aspergillus fumigatus isolates and cryptic species. *J. Antimicrob. Chemother.* **73**, 3063–3067 (2018).

70. Shaw, K. J. & Ibrahim, A. S. Fosmanogepix: A review of the first-in-class broad spectrum agent for the treatment of invasive fungal infections. *J. Fungi* **6**, 239 (2020).

71. Palliyil, S. et al. Monoclonal antibodies targeting surface-exposed Epitopes of Candida albicans cell wall proteins confer in vivo protection in an infection model. *Antimicrob. Agents Chemother.* **66**, e0195721 (2022).

72. Kirui, A. et al. Preparation of fungal and plant materials for structural elucidation using dynamic nuclear polarization solid-state NMR. *J. Vis. Exp.* **144**, e59152 (2019).

73. Liu, Z. et al. Conidium specific polysaccharides in Aspergillus fumigatus. *J. Fungi* **9**, 155 (2023).

74. Johnson, S. B. & Brown, R. E. Simplified derivatization for determining sphingolipid fatty acyl composition by gas chromatography-mass spectrometry. *J. Chromatogr.* **605**, 281–286 (1992).

75. Rienstra, C. M. et al. De novo determination of peptide structure with solid-state magic-angle spinning NMR spectroscopy. *Proc. Natl Acad. Sci. USA* **99**, 10260–10265 (2002).

76. Massiot, D. et al. Modelling one and two-dimensional solid-state NMR spectra. *Magn. Reson. Chem.* **40**, 70–76 (2002).

77. Baldus, M., Petkova, A. T., Herzfeld, J. & Griffin, R. G. Cross polarization in the tilted frame: assignment and spectral simplification in heteronuclear spin systems. *Mol. Phys.* **95**, 1197–1207 (1998).

78. Ader, C. et al. Structural rearrangements of membrane proteins probed by water-edited solid-state NMR. *Spectrosc. J. Am. Chem. Soc.* **131**, 170–176 (2009).

79. White, P. B., Wang, T., Park, Y. B., Cosgrove, D. J. & Hong, M. Water–polysaccharide interactions in the primary cell wall of Arabidopsis thaliana from polarization transfer solid-state NMR. *J. Am. Chem. Soc.* **136**, 10399–10409 (2014).

80. Helmus, J. J. & Jaroniec, C. P. Nmrglue: an open source Python package for the analysis of multidimensional NMR data. *J. Biomol. NMR* **55**, 355–367 (2013).

81. Hunter, J. D. Matplotlib: A 2D graphics environment. *Comput Sci. Eng.* **9**, 90–95 (2007).

82. Wang, T., Williams, J. K., Schmidt-Rohr, K. & Hong, M. Relaxation-compensated difference spin diffusion NMR for detecting 13 C–13 C long-range correlations in proteins and polysaccharides. *J. Biomol. NMR* **61**, 97–107 (2015).

83. Sauvée, C. et al. Highly efficient, water-soluble polarizing agents for dynamic nuclear polarization at high frequency. *Angew. Chem. Int. Ed.* **125**, 11058–11061 (2013).

84. Dubroca, T. et al. A quasi-optical and corrugated waveguide microwave transmission system for simultaneous dynamic nuclear polarization NMR on two separate 14.1 T spectrometers. *J. Magn. Reson.* **289**, 35–44 (2018).

85. De Paëpe, G., Lewandowski, J. R., Loquet, A., Böckmann, A. & Griffin, R. G. Proton assisted recoupling and protein structure determination. *J. Chem. Phys.* **129**, 12B615 (2008).

86. Pauli, J., Baldus, M., van Rossum, B., de Groot, H. & Oschkinat, H. Backbone and Side-chain ^{13}C and ^{15}N signal assignments of the α-Spectrin SH3 domain by magic angle spinning solid-state NMR at 17.6 Tesla. *ChemBioChem* **2**, 272–281 (2001).

87. Wang, T., Salazar, A., Zabotina, O. A. & Hong, M. Structure and dynamics of Brachypodium primary cell wall polysaccharides from two-dimensional ^{13}C solid-state nuclear magnetic Resonance Spectroscopy. *Biochemistry* **53**, 2840–2854 (2014).

88. Addison, B. et al. Atomistic, macromolecular model of the Populus secondary cell wall informed by solid-state NMR. *Sci. Adv.* **10**, adi7965 (2024).

89. Jo, S., Kim, T., Iyer, V. G. & Wonpil, I. CHARMM-GUI: A web-based graphical user interface for CHARMM. *J. Comput. Chem.* **29**, 1859–1865 (2008).

90. Jo, S., Song, K. C., Desaire, H., MacKerell, A. D. & Im, W. Glycan reader: Automated sugar identification and simulation preparation for carbohydrates and glycoproteins. *J. Comput. Chem.* **32**, 3135–3141 (2011).

91. Malaspina, D. C. & Faraudo, J. Chitin builder (v1.0). *Zenodo*, https://doi.org/10.5281/zenodo.3274726 (2019).

92. Humphrey, W., Dalke, A. & Schulten, K. VMD: Visual. *Mol. Dyn. J. Mol. Graph.* **14**, 33–38 (1996).

93. Rinaudo, M. Chitin and chitosan: Properties and applications. *Prog. Polym. Sci.* **31**, 603–632 (2006).

94. Guvench, O., Hatcher, E., Venable, R. M., Pastor, R. W. & MacKerell, A. D. CHARMM additive all-atom force field for glycosidic linkages between Hexopyranoses. *J. Chem. Theory Comput.* **5**, 2353–2370 (2009).

95. Guvench, O. et al. Additive empirical force field for hexopyranose monosaccharides. *J. Comput. Chem.* **29**, 2543–2564 (2008).

96. Jorgensen, W. L., Chandrasekhar, J., Madura, J. D., Impey, R. W. & Klein, M. Comparison of simple potential functions for simulating liquid water. *J. Chem. Phys.* **79**, 926–935 (1983).

97. Beglov, D. & Roux, B. Finite representation of an infinite bulk system: Solvent boundary potential for computer simulations. *J. Chem. Phys.* **100**, 9050–9063 (1994).

98. Essmann, U. et al. A smooth particle mesh Ewald method. *J. Chem. Phys.* **103**, 8577–8593 (1995).

99. Miyamoto, S. & Kollman, P. A. Settle: An analytical version of the SHAKE and RATTLE algorithm for rigid water models. *J. Comput. Chem.* **13**, 952–962 (1992).

100. Paterlini, M. G. & Ferguson, D. M. Constant temperature simulations using the Langevin equation with velocity Verlet integration. *Chem. Phys.* **236**, 243–252 (1998).

101. Feller, S. E., Zhang, Y., Pastor, R. W. & Brooks, B. R. Constant pressure molecular dynamics simulation: The Langevin piston method. *J. Chem. Phys.* **103**, 4613–4621 (1995).

102. Harris & R, C. et al. Array programming with NumPy. *Nature* **585**, 357–362 (2020).

103. Fiorin, G., Klein, M. L. & Henin, J. Using collective variables to drive molecular dynamics simulations. *Mol. Phys.* **111**, 3345–3362 (2013).

104. Latgé, J. P. & Chamilos, G. Aspergillus fumigatus and Aspergillosis in 2019. *Clin. Microbiol. Rev.* **33**, e00140–00118 (2019).

Acknowledgements

Author contributions

M.C.D.W. and I.G. prepared fungal samples. M.C.D.W., I.G. and A.S.L. conducted NMR experiments. I.G. and M.C.D.W. performed the TEM measurements. F.M.V. conducted MAS-DNP experiments. M.C.D.W and I.G. analyzed the NMR, DNP, and TEM data. J.V.V. and D.S. performed MD simulations. S.-Y.D. and I.G. performed the AFM analysis. T.F. and J.P.L. performed the chemical analysis of fungal cell walls. All authors contributed to the writing of the manuscript. P.W. and T.W. designed and supervised the project.

Competing interests

The authors declare no competing interests.

Additional information

Supplementary information The online version contains supplementary material available at https://doi.org/10.1038/s41467-024-50799-8.

Correspondence and requests for materials should be addressed to Tuo Wang.

Peer review information *Nature Communications* thanks Nicolas Minc, David Perlin and the other, anonymous, reviewer for their contribution to the peer review of this work. A peer review file is available.

Reprints and permissions information is available at http://www.nature.com/reprints

Publisher's note Springer Nature remains neutral with regard to jurisdictional claims in published maps and institutional affiliations.